Broad-line region clouds orbiting an AGN sample

J. Armijos-Abendaño [1]★ E. López,[1,2] M. Llerena [3] and C. H. A. Logan[4]

[1] *Observatorio Astronómico de Quito, Escuela Politécnica Nacional, 170136 Quito, Ecuador*
[2] *Departamento de Física, Facultad de Ciencia, Escuela Politécnica Nacional, 170136 Quito, Ecuador*
[3] *Departamento de Física y Astronomía, Universidad de La Serena, Av. Juan Cisternas 1200 Norte, La Serena, Chile*
[4] *HH Wills Physics Laboratory, University of Bristol, Tyndall Avenue, Bristol BS8 1TL, UK*

ABSTRACT

We present a spectral and temporal analysis of *XMM–Newton* data from a sample of six galaxies (NGC 3783, Mrk 279, Mrk 766, NGC 3227, NGC 7314, and NGC 3516). Using the hardness-ratio curves, we identify time intervals in which clouds are eclipsing the central X-ray source in five of the six sources. We detect three occultations in NGC 3227 and one occultation in NGC 3783, NGC 7314, and NGC 3516, together with the well-known occultations in Mrk 766. We estimate the physical properties of the eclipsing clouds. The derived physical size of the X-ray sources ($\sim(3-28) \times 10^{13}$ cm) is less than that of the eclipsing clouds with column densities of $\sim 10^{22}-10^{23}$ cm^{-2}, thus a single cloud may block the X-ray source, leading to notorious temporal variability of the X-ray flux. The eclipsing clouds in Mrk 766, NGC 3227, NGC 7314, and NGC 3516 with distances from the X-ray source of $\sim(0.3-3.6) \times 10^4$ R_g are moving at Keplerian velocities >1122 km s^{-1}, typical parameters of broad-line region clouds, while the eclipsing cloud in NGC 3783 is likely located in the dusty torus. We also find a good anticorrelation with a slope of -187 ± 62 between the known masses of the supermassive black hole in the centre of the galaxies with the equivalent width (EW) of the 6.4 keV Fe line for the five type 1 Seyfert galaxies of our sample, while the type 2 Seyfert galaxy NGC 7314 shows an average EW value of 100 ± 11 eV inconsistent with the above anticorrelation.

Key words: galaxies: active – galaxies: nuclei – X-rays: galaxies.

1 INTRODUCTION

Absorption-driven X-ray variability detected in active galactic nuclei (AGNs) has been interpreted as the passage of absorbing clouds, occulting the central X-ray source (e.g. Risaliti et al. 2011; Torricelli-Ciamponi et al. 2014). Absorption features are expected in the ultraviolet and X-ray spectra when a large cloud or a group of small clouds crosses our line of sight (Bianchi et al. 2009; Wang et al. 2012). The absorbing clouds seem to have properties (locations and scales) similar to those of the emitting clouds of the broad-line region (BLR), so the ultraviolet and X-ray absorbing clouds may be the clouds known as the BLR clouds. Strong absorption-driven variability is expected when low ionization absorbers with neutral cores are eclipsing the central X-ray source (Gaskell 2009; Risaliti et al. 2011). In this case, the iron absorption lines are physically associated with the absorber (Risaliti et al. 2011). The BLR, with a size between $\sim 10^{-4}$ and 0.1 pc (Pietrini, Torricelli-Ciamponi & Risaliti 2019), is illuminated by the photoionizing continuum radiation of the AGN, reprocessing it into emission lines (Gaskell 2009). The cloud geometry is unknown, but it is expected to be irregular. The cloud sizes, determined by different methods, are of the order of $10^{12}-10^{14}$ cm (Risaliti et al. 2011; Pietrini et al. 2019). It has been proposed that the BLR gas may be moving on inflowing or outflowing elliptical trajectories (Williams et al. 2018). Khajenabi (2015) showed that the BLR clouds may be distributed in a disc-like

configuration in AGNs. There is also a hypothesis that the BLR is formed by dusty clouds transferred to regions above the plane of the accretion disc by radiation pressure (Czerny & Hryniewicz 2011).

The column density N_H and the covering factor C_F of the clouds vary proportionally during the occultation, so that an increment of these parameters indicates the occurrence of an occultation of the X-ray source by a cloud (or clouds), which is absorbing/reflecting radiation (Torricelli-Ciamponi et al. 2014). Therefore, the absorption-driven X-ray variability of the source is interpreted as the change of the absorbing column density along the line of sight due to occultation by clouds in the BLR, with about the same size as the X-ray source (Risaliti et al. 2009). It is acceptable to think that the coverage time of the source depends on the cloud size and its velocity. Occultation events in AGNs together with the geometrical and kinematical parameters of eclipsing clouds have been studied before (e.g. Risaliti et al. 2009, 2011; Torricelli-Ciamponi et al. 2014).

BLR models describe the geometry and physical conditions in the line-emitting region of AGNs (Elvis 2017; Williams et al. 2018; Matthews et al. 2020). The broad emission lines may originate in cool clouds ($T \sim 10^4-10^5$ K; e.g. Mathews & Doane 1990; Kuncic, Blackman & Rees 1996). The cool clouds are considered magnetically confined and in thermal equilibrium, in order to explain their long survival times (Kuncic, Celotti & Rees 1997).

Considering the standard AGN model, it is thought that the supermassive black hole (SMBH) is surrounded by an accretion disc and a dusty torus, and that the BLR clouds move in Keplerian orbits inside the dusty torus (Goad, Korista & Ruff 2012; Müller &

★ E-mail: jarmijos090@gmail.com

Table 1. Observational parameters of the studied galaxies.

Galaxy	Type	Distance (Mpc)	ObsIDs	Exposure time ($\times 10^3$ s)
NGC 3783	Seyfert 1	41.6	0780860901	115.0
			0780861001	57.0
Mrk 279	Seyfert 1	131.7	0302480401	59.8
			0302480501	59.8
			0302480601	38.2
Mrk 766	Seyfert 1	64.9	0304030101	95.5
			0304030301	98.9
			0304030401	98.9
NGC 3227	Seyfert 1	22.4	0782520201	92.0
			0782520301	74.0
			0782520401	84.0
			0782520501	87.0
NGC 7314	Seyfert 2	15.8	0725200101	140.5
			0725200301	132.1
NGC 3516	Seyfert 1	38.9	0401210401	52.2
			0401210501	69.1
			0401210601	68.5
			0401211001	68.6

Romero [2020]), while narrow-line region (NLR) clouds are external to the dusty torus (Netzer [2015]). In addition, it is expected we only observe NLRs towards type 2 Seyfert (Seyfert 2) galaxies as the torus obscures the BLRs. On the other hand, both NLRs and BLRs would be observed toward type 1 Seyfert (Seyfert 1) galaxies as the system is more face-on relative to the observer.

X-ray variability of the Seyfert 1 galaxies that we will consider in our study has been studied by Turner et al. ([1999]), who proposed that differences in the mass of the SMBH and the accretion rate could explain the X-ray variability in the studied AGNs, but differences in the physical conditions and geometry of the circumnuclear gas can also be invoked to explain the observed X-ray variability.

This study aims to identify the presence of cloud occultations of the central X-ray source in six AGNs (see Table [1]) by using the hardness-ratio (HR) light curves, as well as to characterize the physical properties of the clouds eclipsing the central X-ray source. For our study, we selected five Seyfert 1 galaxies since it is more likely to observe BLRs towards this type of galaxies. We have also included one Seyfert 2 galaxy (NGC 7314) in our sample to find possible differences in the derived parameters of the Seyfert 1 galaxies with those of the Seyfert 2 galaxy. Here, we study the physical properties of BLR clouds following the methods used by Risaliti et al. ([2007], [2011]). As far as we are aware, these methods have not been used before to study BLR clouds of our sample of galaxies, except for Mrk 766 (included in our study to check part of our results and for comparison purposes). Markowitz, Krumpe & Nikutta ([2014]) studied obscuring clouds in NGC 3783 and NGC 3227, proposing that they are located in the dusty torus, but the method used by Markowitz et al. ([2014]) to constrain obscuring cloud locations is different from those used by Risaliti et al. ([2007], [2011]). The objects presented in this contribution are only a small sample, which will be larger in future research. Nevertheless, we suggest the results from this work provide important new insight into the AGN obscuring phenomenon. In Section [2], we describe the observations and data reduction. In Section [3], we present the results of temporal and spectral analysis of the X-ray data. In Section [4], we discuss the relation found between the equivalent width (EW) of the Fe Kα line at 6.4 keV and the mass

of the SMBH, as well as the physical properties of the eclipsing clouds. Finally, in Section [5], we report the conclusions of this study.

2 OBSERVATIONS AND DATA REDUCTION

The *XMM–Newton* space mission has made many observations of Seyfert galaxies, and a large data base is available through the *XMM–Newton* Science Archive.[1] We selected a sample of six galaxies from this archive with long observations times of at least ∼40 ks, which is necessary to see changes in the HR light curves of the galaxies and thus identify possible occultations of the central X-ray source (see below). These galaxies are also selected for our study as the mass of the SMBHs is known and changes within ∼(1–80) × 10^6 M$_\odot$ (Onken & Peterson [2002]; Onken et al. [2003]; Giacchè, Gilli & Titarchuk [2014]; Piotrovich et al. [2015]; Emmanoulopoulos et al. [2016]), which will allow us to find possible relations between the mass of SMBHs with derived parameters. This is a pilot project that will be extended to other galaxies with high redshift z, in forthcoming research. The selected data were observed with the European Photon Imaging Camera (EPIC) instrument. The Seyfert type, distance, observation ID, and the exposure time are given in Table [1], for each galaxy. The EPPROC task of the Science Analysis Software[2] (SAS, version 19.1.0) was used to run the default pipeline processing, thus obtaining the calibrated event lists. We then used the EVSELECT task of SAS for filtering the data, as well as for extracting light curves and spectra toward the central regions of the galaxies. Fig. [1] shows the X-ray emission maps of the six galaxies. We selected a region free from contamination sources for the background of each galaxy. We used the same radius size of the source for the background regions.

We have studied the X-ray emission arising in the central circular regions with a radius of 21 arcsec for NGC 7314, 25 arcsec for NGC 3783, NGC 279, Mrk 766, and 29 arcsec for NGC 3516 (see Fig. [1]). These galaxies are nearby sources with redshifts within 0.004–0.031 and bright with 2–10 keV fluxes within ∼(1–5) × 10^{-11} erg cm^{-2} s^{-1} (see below), so the above source radii can be adopted for our study. As mentioned above, five of the studied galaxies are Seyfert 1, so the detection of eclipsing events is expected, while the Seyfert 2 galaxy is included in this study for comparative purposes.

## 3 ANALYSIS OF THE X-RAY DATA

3.1 Temporal analysis

We show the 1–10 and 6–10 keV flux light curves in Figs [2–7] for the observations of the six galaxies included in our study. In these figures, we also show the HR light curves (F(6–10)/F(1–5)), which reveal time intervals with strong changes in the X-ray radiation, likely originating as a consequence of occultations of the central X-ray source by clouds crossing the line of sight. As mentioned above, for this analysis we extracted data towards the circular region of the six galaxies.

In Fig. [2], the time interval 1 shows a strong change[3] in the HR light curve in NGC 3783. None of the studied time intervals show

---

[1]http://nxsa.esac.esa.int/nxsa-web/#search
[2]See https://www.cosmos.esa.int/web/xmm-newton/sas
[3]In this paper, we consider a change in the HR light curve when this change is greater than 25 per cent inside the same time interval or there is a change in the HR light curves greater than 25 per cent between time intervals.
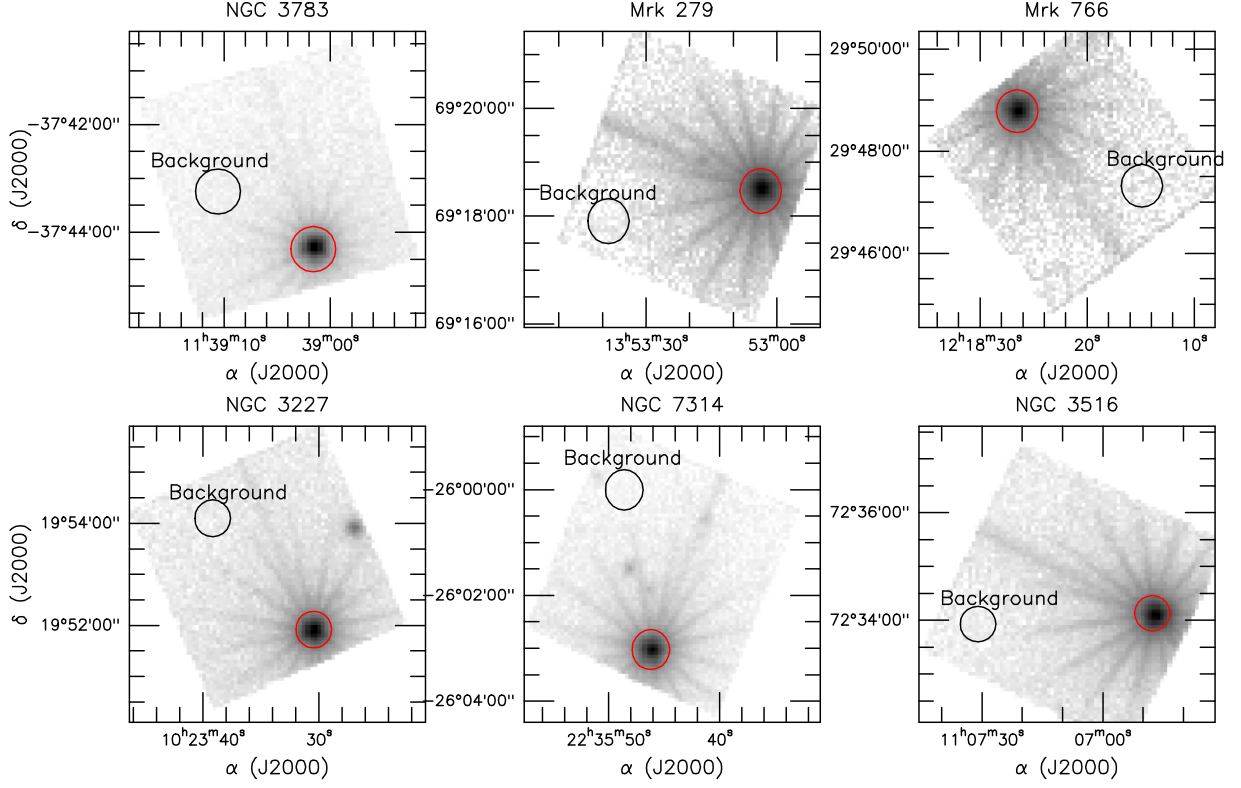
Figure 1. 1–10 keV band maps of the six AGNs studied in this paper. The black circle shows the region used as background, while the red circle shows the region used to extract spectra and light curves for each galaxy.
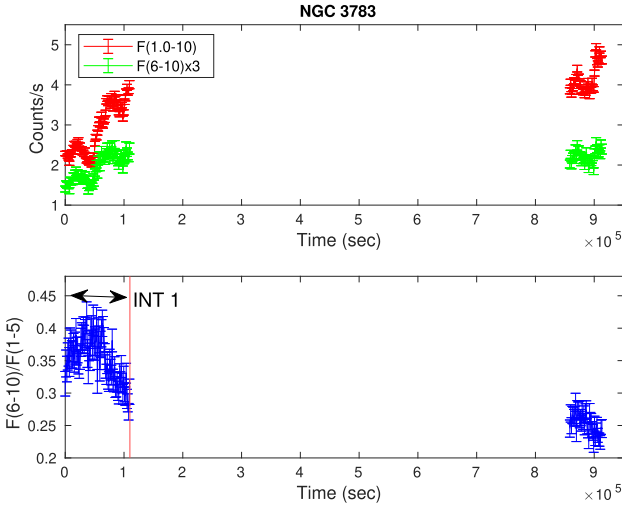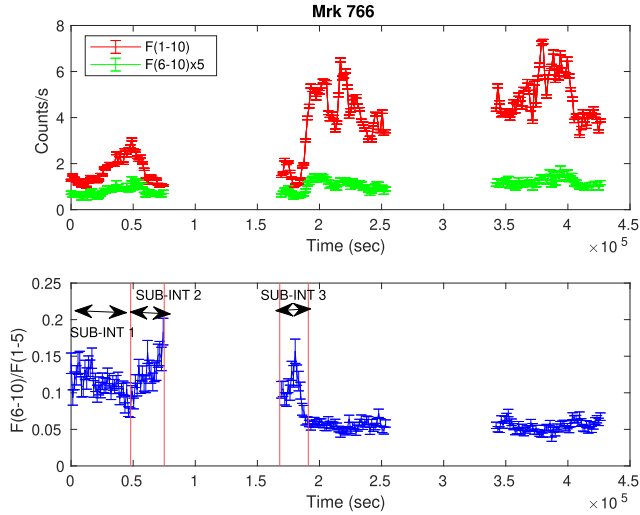

Figure 2. The 1–10 and 6–10 keV flux light curves (top panel) and HR (bottom panel) of NGC 3783. The time interval 1 showing a change in the HR is indicated.
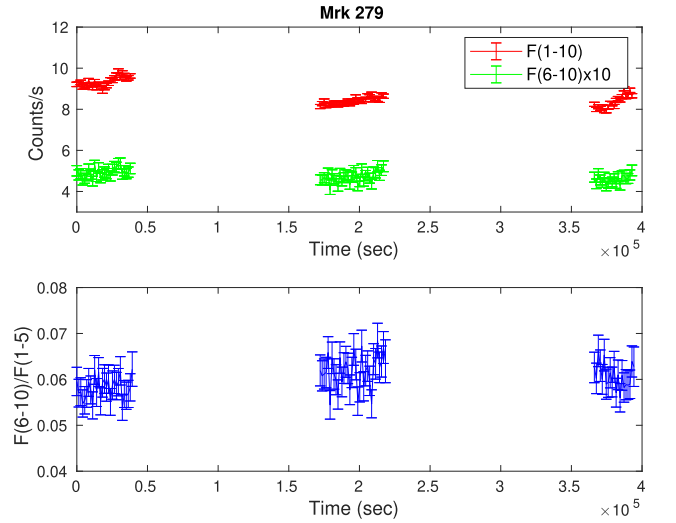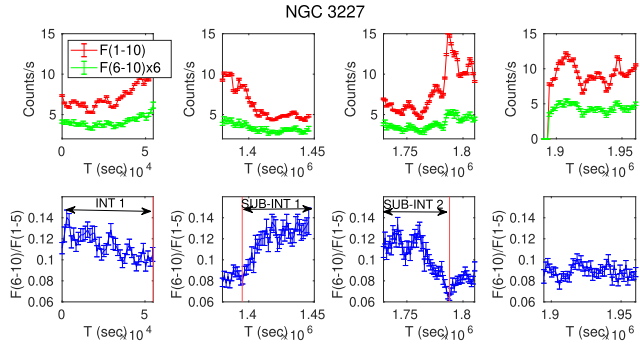

Figure 3. The 1–10 and 6–10 keV flux light curves (top panel) and HR (bottom panel) of Mrk 279.

changes in the HR curves in Mrk 279 (see Fig. 3). The time intervals 1–2 reveal strong changes in the HR curves in Mrk 766 (see Fig. 4). We have labelled three time subintervals as SUB-INT 1, SUB-INT 2, and SUB-INT 3 in Fig. 4, where changes in the HR light curves of Mrk 766 are observed. These time intervals were studied in detail by Risaliti et al. (2011). As mentioned above, we included Mrk 766 in our study for verifying part of the results with those of Risaliti et al. (2011). The time interval 1 and time subintervals SUB-INT 1 and SUB-INT 2 show variations in the HR light curves in NGC 3227

(see Fig. 5). For NGC 7314 (see Fig. 6), the time subinterval labelled as SUB-INT 1 shows a change in the HR curve. We notice in Fig. 7 a change in the HR light curve of the time interval 3 in NGC 3516. In summary, NGC 3783, Mrk 766, NGC 3227, NGC 7314, and NGC 3516 show changes in their HR curves, which could be a consequence of occultations of the central X-ray source by orbiting clouds. The HR changes evidence the possible occurrence of three cloud occultations in Mrk 766 (already discovered by Risaliti et al.
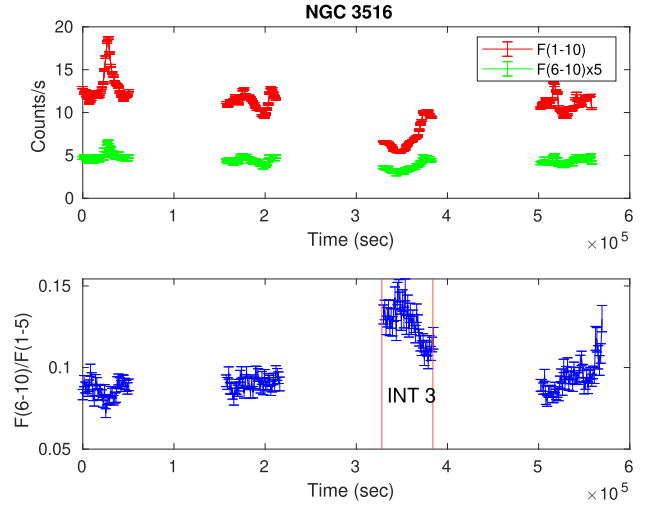
Figure 4. The 1–10 and 6–10 keV flux light curves (top panel) and HR (bottom panel) of Mrk 766. The subintervals 1–3 showing a change in the HR are indicated.

Figure 5. The 1–10 and 6–10 keV flux light curves (top panels) and HR (bottom panels) of NGC 3227. The interval 1 and subintervals 1–2 showing a change in the HR are indicated.
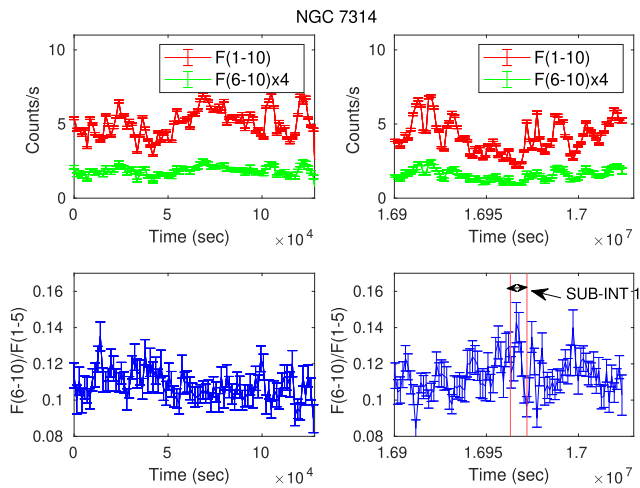
Figure 6. The 1–10 and 6–10 keV flux light curves (top panels) and HR (bottom panels) of NGC 7314. The subinterval 1 showing a change in the HR is indicated.

Figure 7. The 1–10 and 6–10 keV flux light curves (top panels) and HR (bottom panels) of NGC 3516. The time interval 3 showing a change in the HR is indicated.

2011) and NGC 3227, and one cloud occultation in NGC 3783, NGC 7314, and NGC 3516.

To see the possible effects of the soft X-ray emission (0.5–1 keV) on the ratio of the light curves, we show in Figs 8 and 9 the $F(6\text{–}10\text{ keV})/F(0.7\text{–}1\text{ keV})$ curve and the $F(0.7\text{–}1\text{ keV})/F(0.5\text{–}0.7\text{ keV})$ curve. In these figures, we notice that the shape of the $F(6\text{–}10\text{ keV})/F(0.7\text{–}1\text{ keV})$ curves is quite similar to that of the $F(6\text{–}10\text{ keV})/F(5\text{–}1\text{ keV})$ curves shown in Figs 2–7. However, we find differences between the $F(0.7\text{–}1\text{ keV})/F(0.5\text{–}0.7\text{ keV})$ curves and the $F(6\text{–}10\text{ keV})/F(0.7\text{–}1\text{ keV})$ curves in NGC 3783, Mrk 766, NGC 3227, and NGC 3516 (see Figs 8 and 9). The $F(0.7\text{–}1\text{ keV})/F(0.5\text{–}0.7\text{ keV})$ curves do not show changes as those shown by the $F(6\text{–}10\text{ keV})/F(0.7\text{–}1\text{ keV})$ curves in NGC 3227 and NGC 3516 (top and bottom panels in Fig. 9). There is an inversion in the shape of the curves of the SUB-INT 1, SUB-INT 2, and SUB-INT 3 relative to the curve of the third time interval in Mrk 766 (see the bottom panel in Fig. 8). The shape of the $F(0.7\text{–}1\text{ keV})/F(0.5\text{–}0.7\text{ keV})$ curve in NGC 3783 is flatter than that of $F(6\text{–}10\text{ keV})/F(0.7\text{–}1\text{ keV})$. There are no differences in the shape of the curves of Mrk 279 shown in the middle panel of Fig. 8. The $F(0.7\text{–}1\text{ keV})/F(0.5\text{–}0.7\text{ keV})$ curve is noisier than that of $F(6\text{–}10\text{ keV})/F(0.7\text{–}1\text{ keV})$ in NGC 7314, which does not allow us to see the occurrence of possible eclipsing events (see the middle panel of Fig. 9). The fact that the $F(0.7\text{–}1\text{ keV})/F(0.5\text{–}0.7\text{ keV})$ curve does not show the occurrence of eclipsing events in NGC 3227 and NGC 3516, and that this curve is flatter than that of $F(6\text{–}10\text{ keV})/F(0.7\text{–}1\text{ keV})$ in NGC 3783 suggests that the eclipsing events are best observed in the hard X-ray band (>1 keV).

In the following section, we show a spectral analysis for the whole time intervals, as well as a time-resolved analysis of the intervals or subintervals showing variations in the HR $F(6\text{–}10\text{ keV})/F(1\text{–}5\text{ keV})$ curve.

3.2 Spectral analysis

For this analysis, we have used spectra extracted towards the same central regions used for the temporal analysis. A sample of the spectra corresponding to the first time interval for each galaxy is shown in Fig. 10.
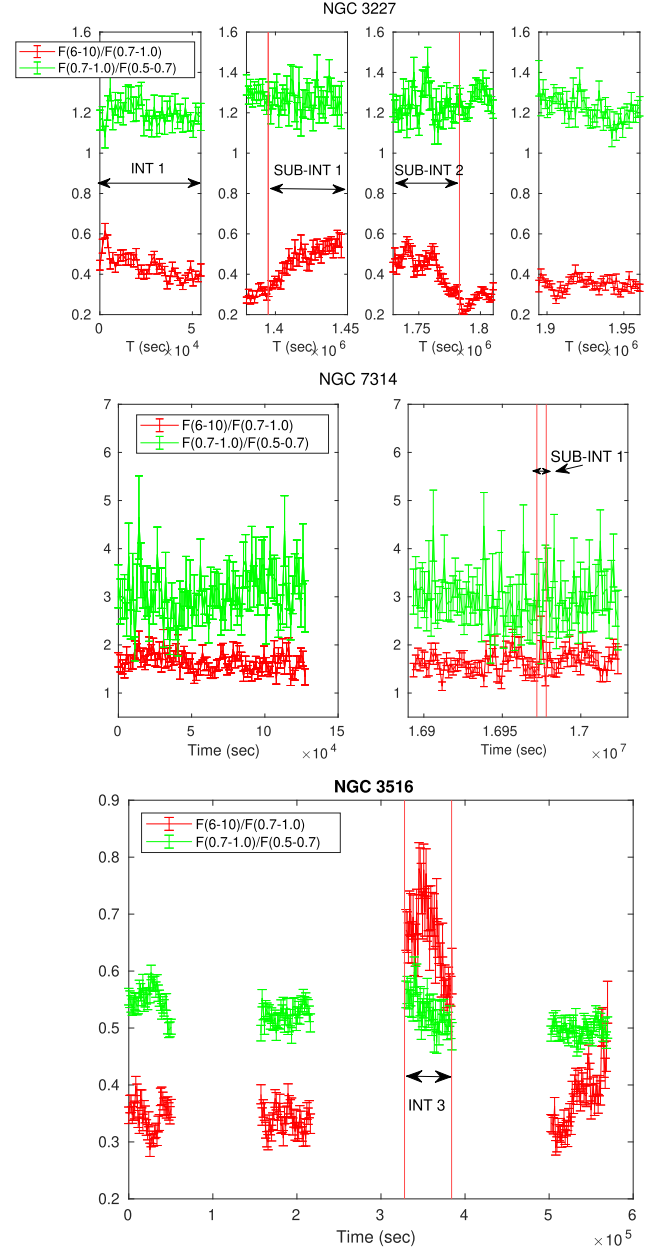
Using XSPEC v12.12.0 (Arnaud 1996), we modelled the spectra considering a partial absorber with free column density (N_H) and
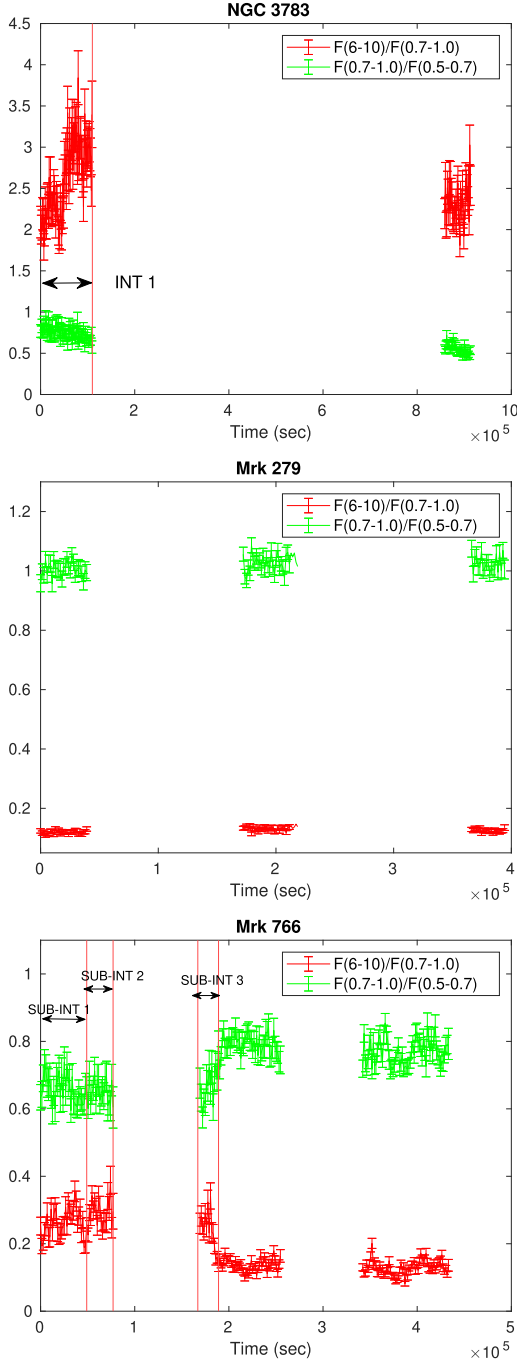
Figure 8. The curves of the 6–10 keV flux over the 0.7–1.0 keV flux (red) and the 0.7–1.0 keV flux over the 0.5–0.7 keV flux (green) for NGC 3783, Mrk 279, and Mrk 766 from the top to the bottom. Different intervals or subintervals showing a change in the HR $F(6–10\ \mathrm{keV})/F(1–5\ \mathrm{keV})$ are indicated for NGC 3783 and Mrk 766.

Figure 9. The curves of the 6–10 keV flux over the 0.7–1.0 keV flux (red) and the 0.7–1.0 keV flux over the 0.5–0.7 keV flux (green) for NGC 3227, NGC 7314, and NGC 3516 from the top to the bottom. Different intervals or subintervals showing a change in the HR $F(6–10\ \mathrm{keV})/F(1–5\ \mathrm{keV})$ are indicated for NGC 3227, NGC 7314, and NGC 3516.

covering fraction (C_F), one Gaussian emission line at 6.4 keV, and a power-law continuum. The N_H and C_F components are included in our modelling as we are interested in studying changes in these two parameters of the absorbers that could be eclipsing the central X-ray source. Our best-fitting models are indicated in Fig. 10 and the estimated parameters are listed in Table 2. The above model allowed us to fit well the spectra of the six galaxies – we obtained a reduced χ^2 within ~0.9–1.2. An additional Gaussian line is needed to fit the

data of NGC 3783, which is fixed at 6.15 keV and has a EW of ~250 eV. This additional line was also used by Blustin et al. (2002) to fit the broad component of the neutral Fe Kα line of NGC 3783. We have a better fit of the spectrum from time interval 1 for NGC 3783, considering an absorption line at ~6.7 keV with a full width at half-maximum (FWHM) of 33 eV. Furthermore, we introduced an absorption feature at ~7.15 keV with an FWHM within 260–310 eV to obtain a better fit of the spectra for the three time intervals in Mrk 766. The presence of absorption features only in NGC 3783 and Mrk 766 may indicate that the absorber in these two galaxies has a lower ionization degree than in the other galaxies included in our study,
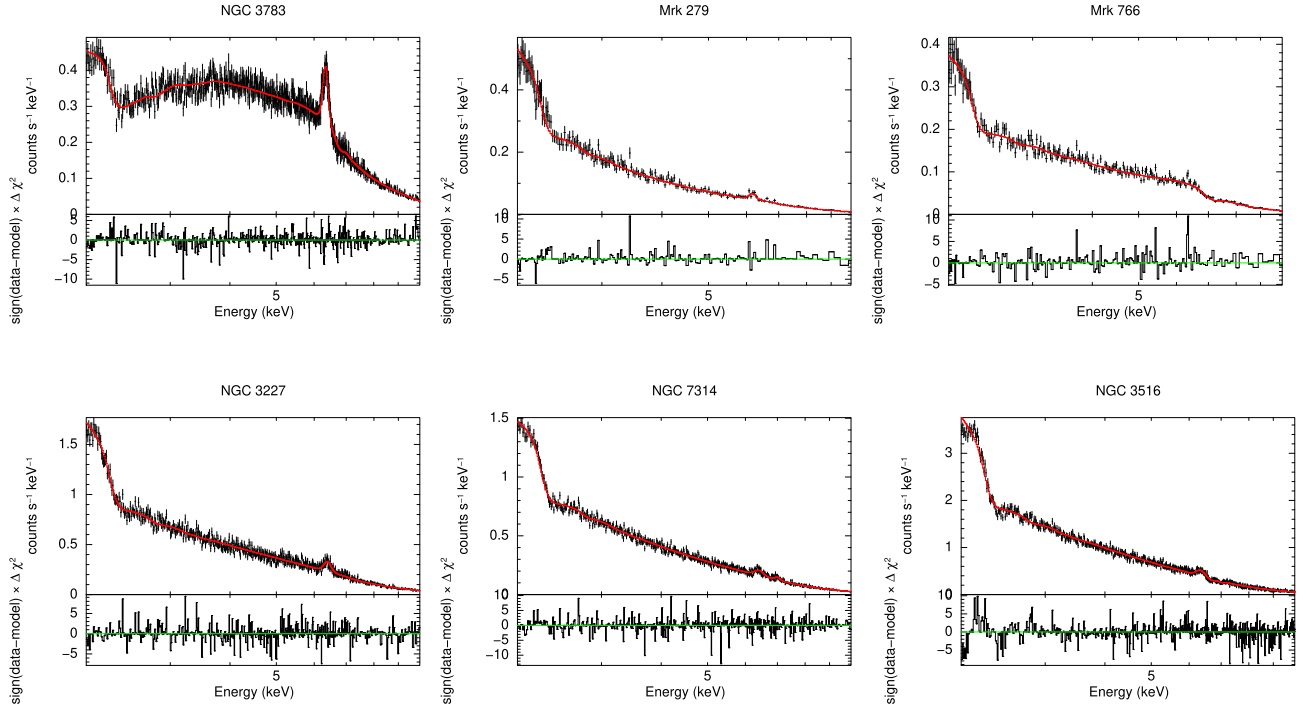
Figure 10. The top panels in each plot show spectra for our sample of AGNs together with the best-fitting models (red line) for the first time interval indicated in Table 1. The bottom panels in each plot show the contribution to the χ^2 value with sign according to the difference of the data and the model for each data point.

which is suggested by Wang et al. (2012) as an important parameter affecting the X-ray absorption. On the other hand, an additional Gaussian line at ∼7 keV is required to fit the hydrogen-like Fe Kα line in the spectra of the Seyfert 2 galaxy NGC 7314. In the next section, we will study the spectra showing changes in the HR curves by considering shorter time-scales.

We also modelled the spectra of the three time intervals for Mrk 279 and Mrk 766 considering the above components plus the PEXRAV model (Magdziarz & Zdziarski 1995) to account for neutral reflection. We modelled the spectrum of the three time intervals of both galaxies keeping all the parameters free. The parameters obtained with this analysis are given in Table 3. We notice that there is very little difference between the parameters listed in Table 2 and those obtained using the PEXRAV component. Therefore, in this paper, we will consider models without the PEXRAV component, for simplicity.

We have presented the averaged value of the EW of the Fe Kα line as a function of the mass of the SMBH in Fig. 11, where the SMBH mass of the Seyfert 1 galaxies and NGC 7314 are taken from Bentz & Katz (2015) and Emmanoulopoulos et al. (2016), respectively. In Fig. 11, we also show a high SMBH mass of $2 \times 10^7 \, M_\odot$ for NGC 3227 (labelled as NGC 3227* in Fig. 11) found by Hicks & Malkan (2008). As can be seen in this figure, it appears that the EW is well anticorrelated with the mass of the SMBH when we consider the high SMBH mass for NGC 3227. The Seyfert 1 galaxies in Fig. 11 follow a linear decreasing relationship, while the EW value of the Seyfert 2 galaxy (NGC 7314) is an outlier outside this relationship, which will be discussed later. To study the dependence between the variables (excluding the Seyfert 2 galaxy), we calculated the Pearson's coefficient and use the least-squares regression taking into account the low (case a) and high (case b) mass estimate of the SMBH for NGC 3227. The Pearson's coefficient was calculated using the PYTHON routine PEARSONR of SCIPY, while the regression

was estimated with the LMFIT package.[4] Thus, we found the following regression for the relation between the EW and the mass of the SMBH in the case a:

$$EW \,(\mathrm{eV}) = (-80.59 \pm 33.39) \log(M_{\mathrm{BH}} \,(10^6 \, M_\odot)) + (712.00 \pm 240.95); \qquad (1)$$

and in the case b:

$$EW \,(\mathrm{eV}) = (-187.25 \pm 62.25) \log(M_{\mathrm{BH}} \,(10^6 \, M_\odot)) + (1491.54 \pm 452.98). \qquad (2)$$

The above relations for the cases a and b are indicated with a blue line and red line, respectively, in Fig. 11. We estimated the Pearson's coefficient of -0.48 and -0.87 for the anticorrelation between the logarithm of the SMBH mass and the EW in the cases a and b, respectively. The above relations have a *p*-value of 0.41 in the case a and 0.059 in the case b. Therefore, there is a better anticorrelation between the two variables in the case b than in the case a.

3.3 Time-resolved analysis

In this section, we analyse the spectra of the time intervals or time subintervals showing changes in the HR curves (see Figs 2 and 4–7) considering short time-scales that allow us to identify changes in the relative flux, N_{H}, and C_{F}. For this, we use uniform time bins and include a number of counts that are large enough for resolving changes in N_{H} and C_{F}, using our models. We focus our spectral analysis on the hard X-ray emission (>1 keV) because, as indicated in Section 3.1, NGC 3227 and NGC 3516 do not

---

[4]https://lmfit.github.io/lmfit-py/intro.html

Table 2. Spectral analysis parameters.

Galaxy	Interval	Γ^a	$N_H{}^b$ ($\times 10^{22}$ cm^{-2})	$C_F{}^c$	Energy^d (keV)	EW^e (eV)	F(2–10 keV)^f ($\times 10^{-11}$ erg s^{-1} cm^{-2})	χ^2/degrees of freedom
NGC 3783	1	1.61 ± 0.02	$8.61^{+0.26}_{-0.25}$	0.83 ± 0.01	$6.42^{+0.01}_{-0.01}$	156^{+17}_{-20}	2.41 ± 0.01	799/787
	2	1.77 ± 0.01	$8.08^{+0.38}_{-0.37}$	0.76 ± 0.01	$6.40^{+0.01}_{-0.01}$	144^{+28}_{-27}	3.00 ± 0.02	760/753
Mrk 279	1	1.97 ± 0.06	$33.06^{+35.33}_{-11.09}$	0.20 ± 0.03	$6.42^{+0.02}_{-0.03}$	82^{+20}_{-20}	2.68 ± 0.02	617/657
	2	1.94 ± 0.05	$119.13^{+59.88}_{-29.51}$	0.34 ± 0.04	$6.37^{+0.04}_{-0.04}$	102^{+41}_{-43}	2.35 ± 0.03	416/441
	3	1.97 ± 0.06	$98.60^{+43.65}_{-22.99}$	0.30 ± 0.02	$6.40^{+0.04}_{-0.13}$	83^{+43}_{-41}	2.36 ± 0.04	324/344
Mrk 766	1	1.91 ± 0.10	$11.10^{+1.26}_{-1.13}$	0.56 ± 0.01	6.40^g	308^{+86}_{-89}	0.72 ± 0.01	699/591
	2	2.18 ± 0.02	$10.66^{+2.98}_{-2.38}$	0.30 ± 0.01	6.40^g	180^{+66}_{-63}	1.11 ± 0.01	555/572
	3	2.15 ± 0.08	$6.76^{+3.42}_{-2.66}$	0.19 ± 0.04	6.40^g	206^{+71}_{-65}	1.40 ± 0.01	602/608
NGC 3227	1	1.67 ± 0.05	$11.95^{+1.73}_{-1.51}$	0.32 ± 0.01	$6.41^{+0.02}_{-0.02}$	117^{+18}_{-16}	3.13 ± 0.02	795/735
	2	1.60 ± 0.06	$7.70^{+2.95}_{-2.32}$	0.17 ± 0.02	$6.41^{+0.01}_{-0.01}$	146^{+17}_{-17}	2.59 ± 0.02	778/740
	3	1.70 ± 0.01	$16.67^{+4.05}_{-3.09}$	0.19 ± 0.01	$6.39^{+0.02}_{-0.02}$	95^{+15}_{-12}	3.14 ± 0.01	840/769
	4	1.72 ± 0.05	$8.08^{+2.94}_{-3.54}$	0.16 ± 0.05	$6.41^{+0.02}_{-0.01}$	111^{+15}_{-15}	3.69 ± 0.02	819/766
NGC 7314	1	1.81 ± 0.01	$1.35^{+0.78}_{-0.38}$	0.68 ± 0.02	$6.44^{+0.02}_{-0.03}$	86^{+13}_{-14}	2.39 ± 0.01	915/782
	2	1.80 ± 0.04	$1.98^{+0.84}_{-0.80}$	0.48 ± 0.22	$6.42^{+0.03}_{-0.03}$	114^{+18}_{-17}	1.99 ± 0.01	841/763
NGC 3516	1	2.03 ± 0.01	$7.37^{+0.56}_{-0.53}$	0.45 ± 0.01	$6.39^{+0.03}_{-0.02}$	89^{+19}_{-20}	5.25 ± 0.02	928/768
	2	2.05 ± 0.01	$7.90^{+0.51}_{-0.48}$	0.48 ± 0.01	$6.37^{+0.02}_{-0.01}$	123^{+15}_{-13}	4.58 ± 0.02	954/766
	3	2.02 ± 0.01	$8.07^{+0.43}_{-0.41}$	0.61 ± 0.01	$6.38^{+0.02}_{-0.01}$	139^{+18}_{-16}	3.56 ± 0.02	864/743
	4	2.05 ± 0.04	$7.13^{+0.73}_{-0.77}$	0.48 ± 0.03	$6.41^{+0.17}_{-0.06}$	133^{+17}_{-15}	4.59 ± 0.02	890/769

[a]Photon index of the continuum. The uncertainties given in this table are at the 90 per cent confidence level for one parameter of interest.
[b]Column density of hydrogen.
[c]Covering factor.
[d]Peak energy of the Fe Kα line.
[e]Equivalent width of the 6.4 Fe Kα line.
[f]The 2–10 keV flux.
[g]Fixed parameter.

**Table 3.** Spectral analysis parameters obtained using PEXRAV.

Galaxy	Interval	Γ^a	$N_H{}^b$ ($\times 10^{22}$ cm^{-2})	$C_F{}^c$	Energy^d (keV)	EW^e (eV)	F(2–10)^f ($\times 10^{-11}$ erg s^{-1} cm^{-2})	χ^2/degrees of freedom
Mrk 279	1	1.99 ± 0.05	$30.76^{+22.19}_{-8.55}$	0.20 ± 0.03	$6.42^{+0.02}_{-0.03}$	80^{+1}_{-4}	2.68 ± 0.02	616/657
	2	1.89 ± 0.13	$111.78^{+28.26}_{-16.38}$	0.40 ± 0.01	$6.37^{+0.04}_{-0.04}$	95^{+23}_{-65}	2.35 ± 0.03	416/436
	3	1.83 ± 0.50	$95.02^{+30.55}_{-18.82}$	0.40 ± 0.01	$6.38^{+0.04}_{-0.04}$	73^{+38}_{-36}	2.36 ± 0.05	322/341
Mrk 766	1	1.91 ± 0.06	$8.03^{+1.10}_{-0.99}$	0.49 ± 0.02	6.40^g	113^{+91}_{-60}	0.72 ± 0.01	694/592
	2	1.91 ± 0.02	$15.48^{+3.84}_{-2.99}$	0.20 ± 0.01	6.40^g	135^{+45}_{-41}	1.11 ± 0.01	555/570
	3	2.07 ± 0.08	$4.07^{+4.35}_{-3.46}$	0.14 ± 0.01	6.40^g	127^{+100}_{-93}	1.40 ± 0.02	600/607

[a]Photon index of the continuum. The uncertainties given in this table are at the 90 per cent confidence level for one parameter of interest.
[b]Column density of hydrogen.
[c]Covering factor.
[d]Peak energy of the Fe Kα line.
[e]Equivalent width of the 6.4 Fe Kα line.
[f]The 2–10 keV flux.
[g]Fixed parameter.

reveal the occurrence of eclipsing events in the F(0.7–1 keV)/F(0.5–0.7 keV) curve, while the F(6–10 keV)/F(0.7–1 keV) curve does that. Another argument supporting the choice of the hard X-ray range in our analysis is the following: considering energies <2 keV in the spectral analysis leads to values of $N_H < 1 \times 10^{22}$ cm^{-2} and values of C_F close to 1 in NGC 3227 and NGC 7314, making it impossible to follow changes in the C_F values. For this analysis, we use the models described in Section 3.2 excluding the PEXRAV

component. The results of our analysis are shown in Table 4 and Figs 12–14, where we use a number followed by a letter for labelling the time bins. The number of the bin corresponds to that of the time interval or the time subinterval. We do not analyse the second time interval of Mrk 766 because this was already done in Risaliti et al. (2011).

We notice that the first time interval in Mrk 766 (see Fig. 12, middle panel), the first and second time intervals in NGC 3227 (see
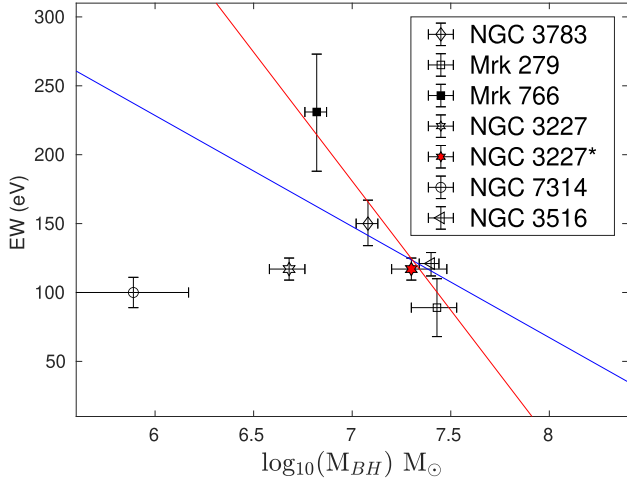
Figure 11. EW of the Fe Kα line as function of SMBH mass, for each galaxy. The red line is the fitted line regression obtained considering NGC 3227 with a $\log_{10}(M_{BH})$ of 7.3 $M_\odot$ (labelled as NGC 3227∗) and the other four Seyfert 1 galaxies, while the blue line is the fitted line regression obtained considering NGC 3227 with a $\log_{10}(M_{BH})$ of 6.7 $M_\odot$ and the other four Seyfert 1 galaxies (see in the text).

Fig. 13, left and middle panels), and the third time interval in NGC 3516 show N_H values with a similar trend to that of the C_F, but the N_H values appear more dispersed (see Fig. 14). The N_H value in the time subinterval 1F of NGC 3227 is out of the trend (see the left-hand panel in Fig. 13), which is not clear. The N_H reveals the highest values in the time subintervals 1B and 1C (within SUB-INT 1) of NGC 7314, where we see the change in the HR light curve (see Fig. 12, right-hand panel), and the lowest value of C_F matches well the lowest value of the HR curve in the SUB-INT 1. The observed trend between N_H and C_F, in the above time intervals or time subintervals of NGC 3227, NGC 7314, and NGC 3516, is consistent with that was found for Mrk 766 by Risaliti et al. (2011), supporting the idea that during the time intervals that show this trend, a cloud or clouds obscure the centre X-ray source. On the other hand, the values of N_H in NGC 3783 show a trend of decreasing with time, while the values of C_F reveal a modest increase. The N_H reaches its maximum value around 1.77×10^6 s and the values of C_F show a clear decrease with time in the third time interval of NGC 3227 (see Fig. 13, right-hand panel). It is not clear why the values of N_H do not follow the values of the C_F in the first time interval of NGC 3783 and the third time interval of NGC 3227, which show changes in the HR curves. We also notice in Figs 12–14 that there is a clear anticorrelation between the HR curve and the relative flux for the studied galaxies, except for NGC 7314. It is difficult to check changes of the relative flux and of the other two parameters in SUB-INT 1 of NGC 7314, because there are only two possible estimates within this time subinterval (see right-hand panel of Fig. 12).

To see the variations in the values of N_H and C_F with time and their uncertainties, Fig. 15 shows contour plots of C_F versus N_H of several representative time intervals given in Table 4. We see in this figure that there are uncertainties with overlapping ranges. We estimate these uncertainties with XSPEC at 68 per cent and 90 per cent confidence levels, which allow us to distinguish the changes in both parameters with time. For example, the values of N_H and C_F tend to increase with time in the second time interval of NGC 3227 (panel e in Fig. 15), while the values of C_F increase and those of N_H decrease with time for the first time interval of NGC 3783 (panel b in Fig. 15).

Table 4. Parameters of the time-resolved spectral analysis.

Galaxy	Inter.	N_H [a] $(\times 10^{22} \text{ cm}^{-2})$	C_F [b]	F/F' [c]	χ^2/degrees of freedom
NGC 3783	1A	$9.12^{+1.60}_{-1.62}$	0.82 ± 0.03	0.61 ± 0.01	397/409
	1B	$9.66^{+0.95}_{-0.93}$	0.79 ± 0.04	0.69 ± 0.01	400/463
	1C	$8.70^{+0.98}_{-1.04}$	0.81 ± 0.02	0.62 ± 0.01	383/389
	1D	$10.67^{+0.86}_{-0.81}$	0.82 ± 0.01	0.64 ± 0.01	380/408
	1E	$8.97^{+0.66}_{-0.70}$	0.85 ± 0.02	0.87 ± 0.02	529/559
	1F	$8.87^{+0.60}_{-0.60}$	0.87 ± 0.01	0.97 ± 0.01	593/565
	1G	$8.55^{+0.64}_{-0.62}$	0.83 ± 0.01	0.94 ± 0.01	536/557
	1H	$8.76^{+1.31}_{-1.05}$	0.86 ± 0.02	0.95 ± 0.01	507/555
Mrk 766	1A	$21.37^{+6.19}_{-4.60}$	0.67 ± 0.02	0.37 ± 0.02	124/108
	1B	$13.49^{+4.67}_{-3.80}$	0.67 ± 0.03	0.40 ± 0.02	109/106
	1C	$11.17^{+2.45}_{-2.24}$	0.76 ± 0.03	0.46 ± 0.02	124/121
	1D	$13.52^{+2.54}_{-2.11}$	0.68 ± 0.02	0.66 ± 0.02	192/174
	2A	$4.00^{+1.87}_{-1.63}$	0.63 ± 0.26	0.68 ± 0.02	230/191
	2B	$8.05^{+3.40}_{-2.71}$	0.52 ± 0.05	0.74 ± 0.02	197/194
	2C	$13.11^{+5.93}_{-4.18}$	0.50 ± 0.04	0.44 ± 0.02	142/153
	2D	$22.02^{+6.35}_{-4.73}$	0.74 ± 0.02	0.37 ± 0.02	118/90
NGC 3227	1A	$13.68^{+5.26}_{-3.70}$	0.36 ± 0.02	0.82 ± 0.02	374/407
	1B	$20.59^{+12.30}_{-7.51}$	0.30 ± 0.02	0.75 ± 0.01	304/353
	1C	$12.62^{+5.80}_{-3.76}$	0.35 ± 0.02	0.70 ± 0.01	371/351
	1D	$10.11^{+3.80}_{-2.85}$	0.36 ± 0.03	0.78 ± 0.01	380/371
	1E	$11.31^{+3.59}_{-2.76}$	0.40 ± 0.02	0.78 ± 0.01	359/371
	1F	$19.91^{+4.51}_{-3.61}$	0.29 ± 0.02	0.93 ± 0.02	371/407
	1G	$7.43^{+9.80}_{-5.40}$	0.11 ± 0.02	1.04 ± 0.02	443/434
	2A	$0.18^{+0.27}_{-0.18}$	0.22 ± 0.28	0.94 ± 0.01	479/474
	2B	$1.40^{+5.60}_{-0.60}$	0.27 ± 0.13	0.85 ± 0.01	456/446
	2C	$3.07^{+6.01}_{-3.03}$	0.17 ± 0.03	0.66 ± 0.01	388/394
	2D	$13.72^{+3.33}_{-2.69}$	0.34 ± 0.02	0.60 ± 0.01	378/364
	2E	$10.67^{+4.35}_{-3.23}$	0.25 ± 0.03	0.56 ± 0.01	335/346
	2F	$13.53^{+2.58}_{-2.48}$	0.25 ± 0.02	0.63 ± 0.01	365/374
	2G	$13.88^{+7.88}_{-5.56}$	0.32 ± 0.04	0.57 ± 0.01	294/318
	3A	$16.02^{+2.79}_{-2.35}$	0.33 ± 0.02	0.73 ± 0.01	471/469
	3B	$12.00^{+1.80}_{-1.52}$	0.30 ± 0.01	0.67 ± 0.01	446/441
	3C	$15.88^{+7.33}_{-4.63}$	0.28 ± 0.01	0.62 ± 0.01	395/427
	3D	$37.52^{+27.00}_{-14.00}$	0.11 ± 0.02	0.75 ± 0.01	416/436
	3E	$30.33^{+6.49}_{-4.99}$	0.22 ± 0.01	0.95 ± 0.01	557/515
	3F	$20.03^{+11.32}_{-7.19}$	0.17 ± 0.02	1.11 ± 0.01	599/545
	3G	$10.52^{+3.04}_{-2.27}$	0.15 ± 0.01	1.05 ± 0.01	479/503
NGC 7314	1A	$2.67^{+4.41}_{-2.02}$	0.35 ± 0.05	0.63 ± 0.01	182/203
	1B	$9.28^{+4.76}_{-3.35}$	0.41 ± 0.05	0.53 ± 0.02	160/173
	1C	$4.93^{+5.78}_{-3.78}$	0.24 ± 0.20	0.63 ± 0.02	220/206
	1D	$3.97^{+3.35}_{-2.64}$	0.42 ± 0.25	0.84 ± 0.02	244/261
	1E	$4.47^{+3.11}_{-2.50}$	0.45 ± 0.20	0.67 ± 0.02	218/220
	1F	$0.60^{+0.12}_{-0.12}$	0.85 ± 0.13	1.04 ± 0.02	288/306
	1G	$1.00^{+0.24}_{-0.23}$	0.65 ± 0.14	0.67 ± 0.02	254/217
NGC 3516	3A	$10.09^{+1.23}_{-1.12}$	0.61 ± 0.02	0.69 ± 0.01	496/456
	3B	$7.64^{+1.19}_{-1.09}$	0.62 ± 0.03	0.62 ± 0.01	429/425
	3C	$6.78^{+1.19}_{-1.08}$	0.62 ± 0.04	0.62 ± 0.01	437/421
	3D	$9.54^{+1.25}_{-1.13}$	0.61 ± 0.02	0.70 ± 0.01	489/456

Table 4 – *continued*

Galaxy	Inter.	N_H [a] $(\times 10^{22} \text{ cm}^{-2})$	C_F [b]	F/F' [c]	χ^2/degrees of freedom
	3E	$7.24^{+1.51}_{-1.63}$	0.63 ± 0.05	0.81 ± 0.01	441/482
	3F	$5.71^{+0.89}_{-0.84}$	0.61 ± 0.04	1.02 ± 0.01	555/532
	3G	$8.43^{+1.01}_{-0.92}$	0.59 ± 0.02	0.97 ± 0.01	580/523
	3H	$6.96^{+1.01}_{-0.92}$	0.58 ± 0.03	1.03 ± 0.01	523/535

Note. Mrk 279 does not show changes in the HR curves, so it does not appear in this table. [a]Column density of hydrogen. The uncertainties given in this table are at the 90 per cent confidence level for one parameter of interest. [b]Covering factor.
[c]Relative flux, which is the 2–10 keV flux normalized to that estimated in the second, third, first, fourth, and fifth time intervals for NGC 3783, Mrk 766, NGC 3227, NGC 7314, and NGC 3516, respectively.

4 DISCUSSION

4.1 Relation between the EW of the 6.4 keV Fe line with the black hole mass

The best anticorrelation between the values of the EW of the Fe Kα line with the SMBH mass is shown in Fig. 11 for the five Seyfert 1 galaxies studied in this paper, which is fitted using the equation (2). On the other hand, the average EW of the Syfert 2 NGC 7314 is not consistent with this relation. NGC 7314 with a SMBH mass of $0.9 \times 10^6 \, M_\odot$ reveals an average EW of 100 ± 11 eV, which is a factor of 2.3 lower than that of Mrk 766 with a SMBH mass of $6.6 \times 10^6 \, M_\odot$. The average EW for NGC 7314, derived in this contribution, is consistent with the 82^{+19}_{-21} eV found by Zoghbi et al. (2013) for the same galaxy. Considering the linear regression in Fig. 11 fitted with equation (2), an EW of ∼380 eV is expected for a Seyfert 1 AGN with a SMBH mass of $0.9 \times 10^6 \, M_\odot$ equal to that of NGC 7314. This contrasts with the findings by Singh, Shastri & Risaliti (2011), who found that the EW values of the Fe Kα line in Seyfert 2 galaxies are higher than in Seyfert 1 galaxies, which could be a consequence of measuring the EW against the depressed continuum by the torus obscuration in Seyfert 2 galaxies (Singh et al. 2011). On the contrary, our findings are consistent with the attenuation in the luminosity of the Fe Kα line in Compton-thick Seyfert 2 galaxies (likely due to absorption of the reflected component) compared to that of Seyfert 1 galaxies with the same mid-infrared (IR) luminosity (Ricci et al. 2014).

Fig. 11 suggests that the SMBH mass can directly affect the Fe Kα line emission region in Seyfert 1 galaxies. The EW–SMBH mass anticorrelation is expected from the EW–X-ray luminosity anticorrelation known as the X-ray Baldwin effect (Iwasawa & Taniguchi 1993; Page et al. 2004; Shu, Yaqoob & Wang 2010). Nandra et al. (1997) found that the Fe Kα line emission in Seyfert 1 galaxies likely originates in the accretion disc orbiting the SMBH. On the other hand, Fukazawa et al. (2011) discovered that the Fe Kα line is likely generated in the Compton-thick torus because they found a relation between the EW of the Fe Kα line and the absorption column density in Seyfert galaxies. The accretion rate, proposed as responsible for producing the X-ray Baldwin effect (Winter et al. 2009), could play an important role in causing the EW–SMBH mass anticorrelation if the Fe Kα emission line is generated in the accretion disc.

4.2 Physical properties of the eclipsing clouds

We analysed with the same procedure described by Risaliti et al. (2011) the X-ray variability of six Seyfert galaxies (see Table 1), including the galaxy Mrk 766 discussed by Risaliti et al. (2011).

These observations were achieved with the *XMM–Newton* mission using the PN instrument. The AGNs are bright enough [$F(2$–$10)$ keV] $\gtrsim 1 \times 10^{-11}$ erg cm^{-2} s^{-1} with a long observation time of at least ∼40 ks. In the same way, we carried out a preliminary analysis of the HR between the high- and low-energy light curves [(6–10 keV)/(1–5 keV)] to identify intervals where the strongest spectral variations of the X-ray radiation take place due to the occultation by the clouds of the BLR. Then, we identified the occultation events and estimated their durations from the HR light curves.

We can estimate the cloud velocity, having information about the eclipse time and the variation of the covering factor during the occultation, using the expression by Risaliti et al. (2011) derived assuming that the central X-ray source has a size of at least $5R_g$: $V > 2.5 \times 10^3 \, M_6 T_4^{-1} \sqrt{\Delta C_F}$ (km s^{-1}), where M_6 is the black hole mass in units of $10^6 \, M_\odot$, T_4 the occultation time in units of 10^4 s, and ΔC_F is the covering factor variation during the eclipse. As we will see below, our sources have sizes much larger than five gravitational radii ($R_g = 2 \frac{G M_{BH}}{c^2}$), so the above expression can be applied undoubtedly. On the other side, considering that the obscuring clouds are moving with Keplerian velocities, and combining the transverse velocity of the clouds with their occultation times derived from the variability of the HR light curves for each galaxy, a geometrical limit on the X-ray source size can be obtained using the expression given by Risaliti et al. (2007): $D_s = (G M_{BH})^{\frac{1}{3}} T^{\frac{2}{3}}$, where M_{BH} is the black hole mass and T is the occultation time. To estimate the size of the eclipsing cloud we consider the distribution of material across the BLR by the covering factor $\frac{\Omega}{4\pi}$, where Ω is the angle subtended by the clouds, so we use the expression $D_c = 4\sqrt{C_F} D_s$.

The physical parameters of the sources and BLR clouds are given in Table 5. We have not included Mrk 279 in Table 5 as this galaxy does not show changes in the HR curves, which is needed for deriving occultation times and variation in the covering factor. This is the reason why we have not included the parameters of some time intervals or time subintervals of the other AGNs in Table 5 either. The derived values in Table 5 for the first and third time intervals of NGC 3783 and NGC 3227, respectively, may be biased because the N_H values do not follow the C_F values, as mentioned above, which is expected when there are gradients in both parameters across the line of sight (see Risaliti et al. 2011). It is noted that at X-ray energies a single cloud can nearly fully block our view of the X-ray source since the cloud is larger than the continuum source (with sizes within ∼$(30$–$100) R_g$). The clouds have linear dimensions of ∼10^{14}–10^{15} cm, velocities >750 km s^{-1}, assuming that the clouds orbit the SMBH with Keplerian velocities, and densities $n_c \sim 10^8$–10^9 cm^{-3}. From our analysis, we found that the column density of eclipsing clouds is about 10^{23} cm^{-2} (except for NGC 7314 with a column density of 2×10^{22} cm^{-2}, see Table 2) and the linear scale of the cloud is of the order of 10^{14} cm, then the corresponding density of the cloud is within 10^8–10^9 cm^{-3} as was indicated above (see Table 5). This is in agreement with the results by Wang et al. (2012), who found that strong X-ray absorption takes place when eclipsing clouds with column densities of 10^{22}–10^{23} cm^{-2} are far from the central black hole, leading to lower ionization degrees and larger opacities of the clouds. As expected from the expressions used in our estimates (the black hole mass is directly proportional to the velocity and size of the cloud), NGC 3516 with a massive black hole of 25 million solar masses evidences the coupling feedback between the central black hole and the surrounding galaxy, making cloud velocities faster and the size of the clouds and the continuum source larger. Assuming Keplerian velocities, we can estimate distances (r_c) of the absorbing clouds from
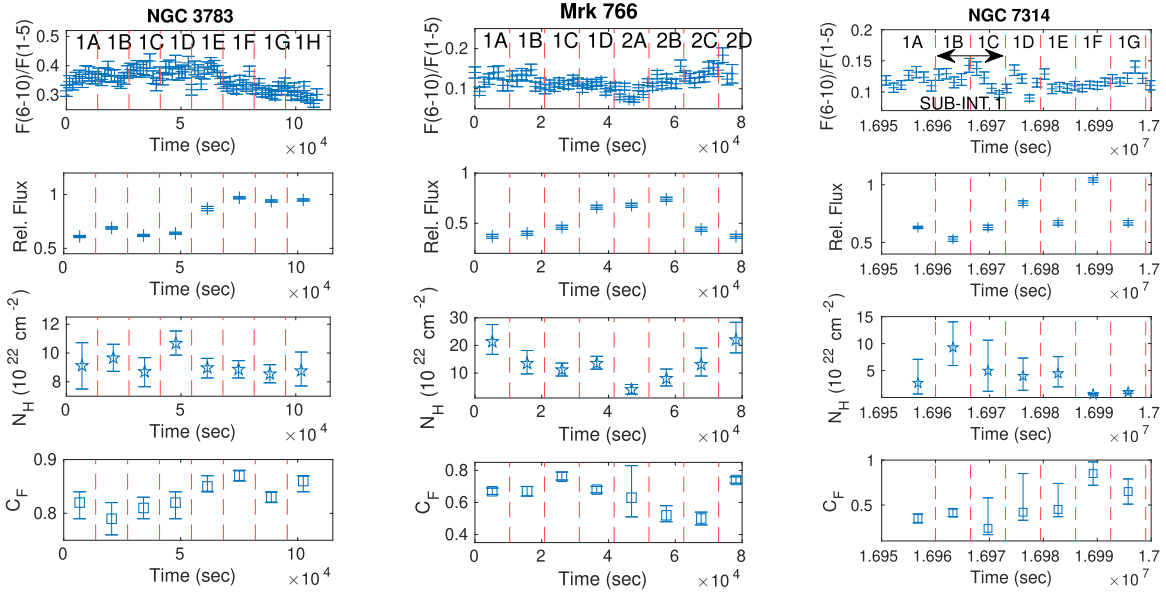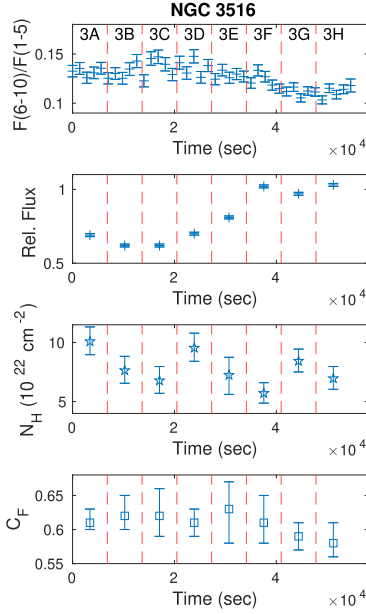
Figure 12. Left-hand panel: the HR, relative flux, column density, and covering factor go from the top to the bottom for NGC 3783 in the first time interval. The relative flux is the 2–10 keV flux normalized to that estimated in the second time interval. Middle panel: as in the left-hand panel but for Mrk 766 in the first time interval and the relative flux is normalized to that in the third time interval. Right-hand panel: as in the left-hand panel but for NGC 7314 in the second time interval and the relative flux is normalized to that in the first time interval.
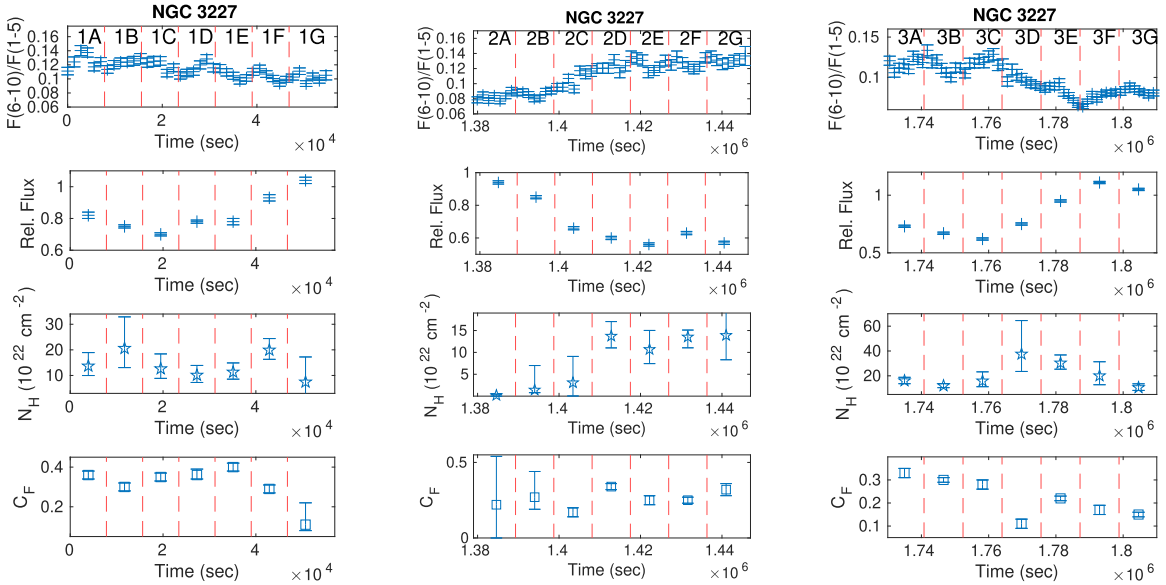
Figure 13. Left-hand panel: the HR, relative flux, column density, and covering factor go from the top to the bottom for NGC 3227 in the first time interval. The relative flux is the 2–10 keV flux normalized to that estimated in the fourth time interval. Middle panel: as in the left-hand panel but for the second time interval. Right panel: as in the left-hand panel but for the third time interval.

the central X-ray source, which are given in the last two columns of Table 5.

The cloud in NGC 3783 shows a velocity >750 km s^{-1} slightly higher than those below 700 km s^{-1} found for the NLR in AGNs (Evans 1988; Rodríguez-Ardila, Contini & Viegas 2005), while the other AGNs reveal cloud velocities >1122 km s^{-1}, so we may be observing a NLR cloud instead of a BLR cloud in NGC 3783. As mentioned above, the cloud velocity derived for NGC 3783 may be biased because the values of N_H do not follow those of C_F

as expected when there are variations in both parameters during an eclipsing event. The high density of 8×10^7 cm^{-3} estimated for NGC 3783 supports the idea that the eclipsing cloud in this AGN is likely a BLR cloud. This density is much larger than those of <10^5 cm^{-3} found for NLRs (Nagao, Maiolino & Marconi 2006).

The changes in HR curves plus the variation trend between the N_H values and the C_F values in Mrk 766, NGC 3227, NGC 7314, and NGC 3516 evidence that BLR clouds are likely eclipsing the

Figure 14. From the top to the bottom: the HR, relative flux, column density, and covering factor for NGC 3516 in the second time interval. The relative flux is the 2–10 keV flux normalized to that estimated in the fourth time interval.

central X-ray sources. The BLR clouds eclipsing the central X-ray source in Mrk 766 were studied in detail in Risaliti et al. (2011). The occultation events observed in NGC 3516 and NGC 3227 are in agreement with the flux variations that could be due to the passage of clumps across the line of sight in NGC 3516 (Turner et al. 2011) and the detection of a transient obscuration event in NGC 3227 (Mehdipour et al. 2021), which would be caused by obscuring winds as opposed to eclipsing clouds. Ebrero et al. (2011) proposed that neutral gas grazing the clumpy torus in NGC 7314 and crossing our line of sight is responsible for the variations in the absorption properties in NGC 7314, which is consistent with our findings but our study shows that the absorber is located in the BLR. De Marco et al. (2020) estimated a density of $>7 \times 10^7$ cm^{-3} for the obscuring gas in the BLR of NGC 3783, which is consistent with the density of the eclipsing cloud found for this galaxy. The column density and the distance (from the central X-ray source) of the eclipsing cloud in NGC 3783 agree with those derived by Reeves et al. (2004) using the absorption line at 6.67 keV, which was also detected in our study (see Section 3.2). Moreover, the column density and covering factor estimated for the eclipsing cloud in NGC 3516 are in agreement with those found by Turner et al. (2008) for an absorber eclipsing the continuum central source in NGC 3516.

The derived distances r_c of the eclipsing clouds from the X-ray source are within $(0.3–8) \times 10^4 R_g$ (see Table 5). The r_c value of $8 \times 10^4 R_g$ derived for NGC 3783 agrees with those of $(7.4–8.6) \times 10^4 R_g$ estimated by Markowitz et al. (2014) for the X-ray absorbing clouds located at the dusty torus of this AGN. The r_c values within $(3–8) \times 10^3 R_g$ derived for Mrk 766 are consistent with those derived by Risaliti et al. (2011) for BLR clouds in this AGN. We find r_c values within $\sim(1–2) \times 10^4 R_g$ for NGC 3227, which are lower than those of $(0.7–2) \times 10^5 R_g$ found for X-ray absorbing clouds located in the dusty torus of this galaxy (Markowitz et al. 2014). We would obtain lower distances around $10^3 R_g$ for the eclipsing clouds in NGC 3227 if we consider the high SMBH mass of 2×10^7 M$_\odot$ used in our analysis in Section 3.2, which are lower than the BLR

cloud distances within $\sim(0.5–7) \times 10^4 R_g$ measured for NGC 3227 (Markowitz et al. 2014). Furthermore, the r_c values of 9.6×10^{15} cm derived for NGC 7314 and of 3.2×10^{16} cm derived for NGC 3516 are consistent with those expected in BLRs of AGNs with a SMBH mass within $\sim(0.1–2) \times 10^7$ M$_\odot$ (see Pietrini et al. 2019). Thus, the clouds obscuring the central X-ray source in Mrk 766, NGC 3227, NGC 7314, and NGC 3516 show r_c values of $(0.3–3.6) \times 10^4 R_g$, typical of BLR clouds.

5 CONCLUSIONS

We carried out the spectral and temporal analysis of X-ray data of six galaxies observed with the *XMM–Newton* telescope, which was needed for deriving the physical parameters of clouds eclipsing the central X-ray source in five of the six galaxies. Using the HR light curves, we identified occultation events towards the central regions of NGC 3783, NGC 3227, NGC 7314, and NGC 3516, as well as corroborated the occultation events in Mrk 766. The physical size of the central X-ray sources ($\sim(3–28) \times 10^{13}$ cm) is less than the size of the eclipsing clouds, thus a single cloud can block the X-ray source and absorb the X-ray spectrum. The eclipsing clouds in Mrk 766, NGC 3227, NGC 7314, and NGC 3516 have large values of the column densities ($\sim10^{22}–10^{23}$ cm^{-2}) and are located at distances of $\sim(0.3–3.6) \times 10^4 R_g$, typical of BLR clouds, leading to the notorious temporal variability of the X-ray flux during the time that the cloud is crossing our line of sight. On the other hand, the cloud obscuring the X-ray source in NGC 3783 is likely located in the dusty torus.

We see that the covering factor changes from object to object and the existence of intervening clouds is a common feature in AGNs. The gas in the BLR, located in the vicinity of the black hole, is moving at Keplerian velocities of >1122 km s^{-1} (excluding the velocity derived for NGC 3783 because toward this source the estimate of the cloud velocity may be biased).

We found a good anticorrelation with a slope of -187 ± 62 between the known mass of the SMBHs with the EW of the 6.4 keV Fe line for the five Seyfert 1 galaxies considering a $\log_{10}(M_{BH}) = 7.3$ M$_\odot$ for NGC 3227 in our statistical analysis. The average value of the EW of NGC 7314, a Seyfert 2, does not agree with the SMBH mass–EW relation found for the five Seyfert 1 galaxies, supporting previous results (Ricci et al. 2014).
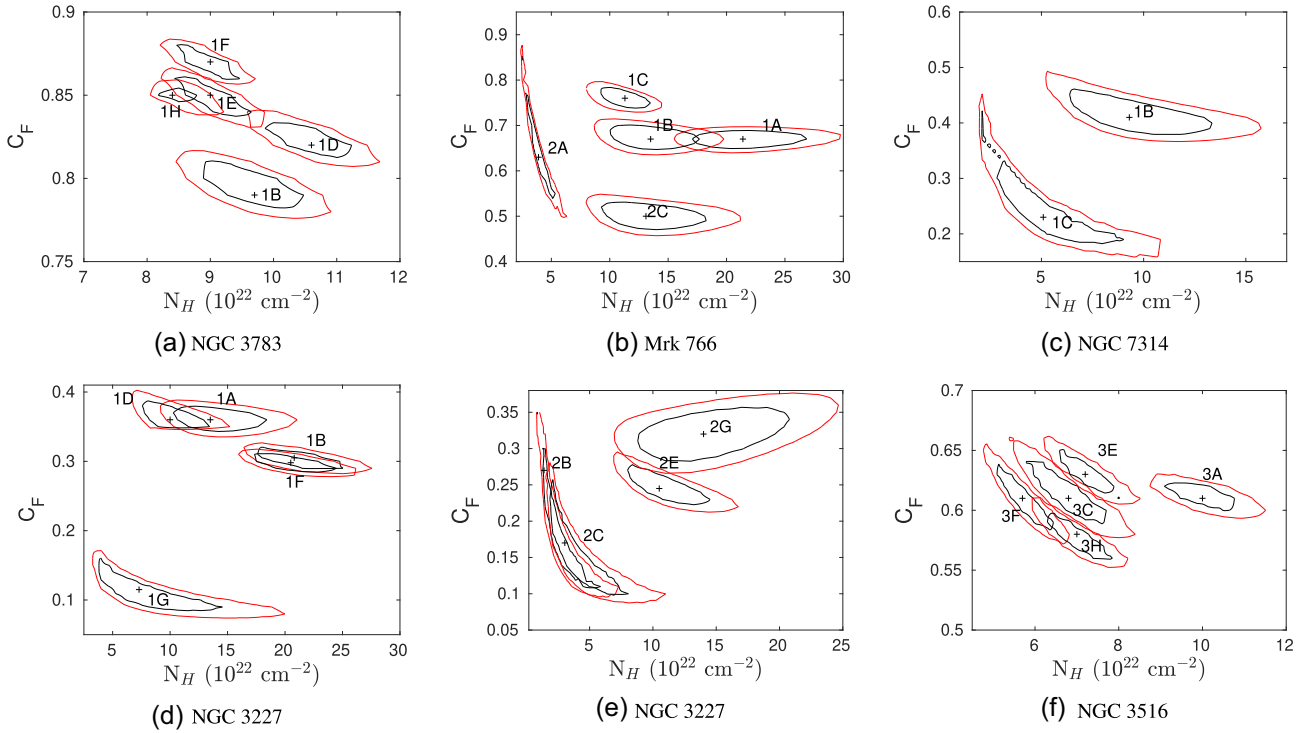
DATA AVAILABILITY

The X-ray data used in this study are accessible from the *XMM–Newton* online archive.[5]

[5]http://nxsa.esac.esa.int/nxsa-web/#search

Figure 15. Contour plots of N_H versus C_F for several representative intervals given in Table 4. The red contours show the 90 per cent confidence level, while the black contours show the 68 per cent confidence level. Labels refer to the time subintervals as defined in Table 4.

Table 5. Derived physical parameters.

Galaxy	Interval or subinterval	M_{BH} [a] $(\times 10^6 \, M_\odot)$	T_4 [b] $(\times 10^4 \, s)$	ΔC_F [c]	V_c [d] $(km \, s^{-1})$	D_s [e] $(\times 10^{13} \, cm)$	D_c [f] $(\times 10^{13} \, cm)$	n_c [g] $(\times 10^8 \, cm^{-3})$	r_c [h] $(\times 10^{15} \, cm)$	r_c [i] $(10^4 \, R_g)$
NGC 3783	1	12.0	12.0	0.09	750	28.5	104.0	0.8	286.0	8.0
Mrk 766	1	6.6	4.0	0.34	2420	11.2	33.7	3.3	15.2	0.8
	2		2.6	0.32	3612	8.4	18.5	5.8	6.8	0.3
NGC 3227	1	4.8	5.4	0.72	1897	12.4	28.0	4.3	18.0	1.2
	2		6.0	0.50	1423	13.3	21.9	3.5	32.0	2.2
	3		4.3	0.49	1966	10.6	18.5	9.0	16.8	1.2
NGC 7314	1	0.9	1.3	0.42	1122	2.7	7.6	2.6	9.6	3.6
NGC 3516	3	25.1	5.5	0.08	3227	21.7	67.7	1.2	32.3	0.4

[a] The SMBH masses are taken from Bentz & Katz (2015) except for NGC 7314 whose SMBH mass is taken from Emmanoulopoulos et al. (2016).
[b] The occultation time.
[c] The covering factor variation during the eclipse.
[d] Velocity of the eclipsing cloud. This value is a lower limit for the velocity.
[e] Size of the central X-ray source.
[f] Size of the eclipsing cloud.
[g] Particle density of the eclipsing cloud.
[h] Distance between the X-ray source and the obscuring cloud.
[i] Distance between the X-ray source and the obscuring cloud in units of R_g.

REFERENCES

Arnaud K. A., 1996, in Jacoby G. H., Barnes J., eds, ASP Conf. Ser. Vol. 101, Astronomical Data Analysis Software and Systems V. Astron. Soc. Pac., San Francisco, p. 17
Bentz M. C., Katz S., 2015, PASP, 127, 67
Bianchi S., Piconcelli E., Chiaberge M., Bailón E. J., Matt G., Fiore F., 2009, ApJ, 695, 781
Blustin A. J., Branduardi-Raymont G., Behar E., Kaastra J. S., Kahn S. M., Page M. J., Sako M., Steenbrugge K. C., 2002, A&A, 392, 453
Czerny B., Hryniewicz K., 2011, A&A, 525, L8

De Marco B. et al., 2020, A&A, 634, A65
Ebrero J., Costantini E., Kaastra J. S., de Marco B., Dadina M., 2011, A&A, 535, A62
Elvis M., 2017, ApJ, 847, 56
Emmanoulopoulos D., McHardy I. M., Vaughan S., Papadakis I. E., 2016, MNRAS, 460, 2413
Evans I. N., 1988, ApJS, 67, 373
Fukazawa Y. et al., 2011, ApJ, 727, 19
Gaskell C. M., 2009, New Astron. Rev., 53, 140
Giacchè S., Gilli R., Titarchuk L., 2014, A&A, 562, A44

Goad M. R., Korista K. T., Ruff A. J., 2012, MNRAS, 426, 3086
Hicks E. K. S., Malkan M. A., 2008, ApJS, 174, 31
Iwasawa K., Taniguchi Y., 1993, ApJ, 413, L15
Khajenabi F., 2015, MNRAS, 446, 1848
Kuncic Z., Blackman E. G., Rees M. J., 1996, MNRAS, 283, 1322
Kuncic Z., Celotti A., Rees M. J., 1997, MNRAS, 284, 717
Magdziarz P., Zdziarski A. A., 1995, MNRAS, 273, 837
Markowitz A. G., Krumpe M., Nikutta R., 2014, MNRAS, 439, 1403
Mathews W. G., Doane J. S., 1990, ApJ, 352, 423
Matthews J. H., Knigge C., Higginbottom N., Long K. S., Sim S. A., Mangham S. W., Parkinson E. J., Hewitt H. A., 2020, MNRAS, 492, 5540
Mehdipour M. et al., 2021, A&A, 652, A150
Müller A. L., Romero G. E., 2020, A&A, 636, A92
Nagao T., Maiolino R., Marconi A., 2006, A&A, 447, 863
Nandra K., George I. M., Mushotzky R. F., Turner T. J., Yaqoob T., 1997, ApJ, 477, 602
Netzer H., 2015, ARA&A, 53, 365
Onken C. A., Peterson B. M., 2002, ApJ, 572, 746
Onken C. A., Peterson B. M., Dietrich M., Robinson A., Salamanca I. M., 2003, ApJ, 585, 121
Page K. L., O'Brien P. T., Reeves J. N., Turner M. J. L., 2004, MNRAS, 347, 316
Pietrini P., Torricelli-Ciamponi G., Risaliti G., 2019, A&A, 628, A26
Piotrovich M. Y., Gnedin Y. N., Silant'ev N. A., Natsvlishvili T. M., Buliga S. D., 2015, MNRAS, 454, 1157

Reeves J. N., Nandra K., George I. M., Pounds K. A., Turner T. J., Yaqoob T., 2004, ApJ, 602, 648
Ricci C., Ueda Y., Paltani S., Ichikawa K., Gandhi P., Awaki H., 2014, MNRAS, 441, 3622
Risaliti G., Elvis M., Fabbiano G., Baldi A., Zezas A., Salvati M., 2007, ApJ, 659, L111
Risaliti G. et al., 2009, MNRAS, 393, L1
Risaliti G., Nardini E., Salvati M., Elvis M., Fabbiano G., Maiolino R., Pietrini P., Torricelli-Ciamponi G., 2011, MNRAS, 410, 1027
Rodríguez-Ardila A., Contini M., Viegas S. M., 2005, MNRAS, 357, 220
Shu X. W., Yaqoob T., Wang J. X., 2010, ApJS, 187, 581
Singh V., Shastri P., Risaliti G., 2011, A&A, 532, A84
Torricelli-Ciamponi G., Pietrini P., Risaliti G., Salvati M., 2014, MNRAS, 442, 2116
Turner T. J., George I. M., Nandra K., Turcan D., 1999, ApJ, 524, 667
Turner T. J., Reeves J. N., Kraemer S. B., Miller L., 2008, A&A, 483, 161
Turner T. J., Miller L., Kraemer S. B., Reeves J. N., 2011, ApJ, 733, 48
Wang Y., Ferland G. J., Hu C., Wang J.-M., Du P., 2012, MNRAS, 424, 2255
Williams P. R. et al., 2018, ApJ, 866, 75
Winter L. M., Mushotzky R. F., Reynolds C. S., Tueller J., 2009, ApJ, 690, 1322
Zoghbi A., Reynolds C., Cackett E. M., Miniutti G., Kara E., Fabian A. C., 2013, ApJ, 767, 121

This paper has been typeset from a TeX/LaTeX file prepared by the author.